Research Article

Fluid properties impact on energy separation in Ranque–Hilsch vortex tube

Ahmad Alsaghir[1] · Mohammad O. Hamdan[1] · Mehmet F. Orhan[1]

© The Author(s) 2022   OPEN

Abstract
This paper examines the energy separation in vortex tubes which is a passive device that can split a pressurized room temperature gas stream to hot and cold streams. The paper employs numerical simulations to investigate the impact of various working fluids such as helium, air, oxygen, nitrogen, and carbon dioxide on the energy separation in the vortex tube, using the SST $k-\omega$ turbulence model with viscous heating. A three-dimensional numerical investigation is sued to examine the effect of a single fluid property on vortex tube performance, while keeping the rest of the fluid properties unchanged, which is impossible to achieve via experimental study. The numerical investigation examines the influence of molecular weight, heat capacity, thermal conductivity, and dynamic viscosity on energy separation. The results show that energy separation performance improves with lower molecular weight and heat capacity, and higher dynamic viscosity of the working fluids, while no impact of the thermal conductivity is observed. Out of five gases tested in this study, helium has yielded the maximum temperature separation, while carbon dioxide has yielded the lowest performance. Results show that viscous dissipation contributes to the temperature separation in vortex tube.

Lis of symbols

Br	Brinkman number, $Br = \mu V^2/(k_f \Delta T)$ (–)
D_ω	Cross diffusion term $[\mathrm{kg/(ms^4)}]$
d	Diameter of inlet nozzle (m)
G_k	Generation of k $[\mathrm{kg/(m.s^3)}]$
G_ω	Generation of ω $[\mathrm{kg/(m.s^4)}]$
k_f	Fluid thermal conductivity $[\mathrm{W/(m.K)}]$
k	Turbulent kinetic energy $[\mathrm{m^2/s^2}]$
L	Vortex tube length $[m]$
L_c	Cold outlet length where outlet cold temperature is measured $[m]$
P_{in}	Inlet pressure [kPa]
Pr	Prandtle number [–]
R	Gas constant [J/kg K]
R_t	Radius of the tube [m]
r_t	Radius of the cold outlet [m]
S_k	User define source term of k $[\mathrm{kg/(m\,s^3)}]$
S_ω	User define source term of ω $[\mathrm{kg/(m\,s^4)}]$
T_{in}	Inlet temperature [K]
T_s	Static temperature [K]
T_t	Total temperature [K]
T	Temperature [K]
V_{in}	Inlet velocity [m/s]
V	Velocity: [m/s]
Y_k	Dissipation of k $[\mathrm{kg/(m\,s^3)}]$
Y_ω	Dissipations of ω $[\mathrm{kg/(m\,s^4)}]$

Greek symbols

Γ_k	Effective diffusivity of k $[\mathrm{kg/(m\,s)}]$
Γ_ω	Effective diffusivity of ω $[\mathrm{kg/(m\,s)}]$
Δ	Change in value
μ	Dynamic viscosity [Pa s]
μ_t	Turbulent viscosity [Pa s]

✉ Mehmet F. Orhan, morhan@aus.edu; Ahmad Alsaghir, b00079096@aus.edu; Mohammad O. Hamdan, mhamdan@aus.edu |
[1]Department of Mechanical Engineering, American University of Sharjah, P.O. Box: 26666, Sharjah, United Arab Emirates.

ρ Density[kg/m^3]
φ Viscous heat generation [(kg K)/(m^3 s)]
ω Specific dissipation [m^2/s^3]

Abbreviations
COP   Coefficient of performance
DV   Dynamic viscosity
HC   Heat capacity
MW   Molecular weight
RHVT   Ranque–Hilsch vortex tube
TC   Thermal conductivity
VT   Vortex tube

1 Introduction

Vortex tube is a mechanical device that enables the instantaneous splitting of a room temperature pressurized fluid stream into low and high temperature streams. It consists of a group of inlet nozzles mounted tangentially on the wall of a circular tube, a cold outlet at the center of the tube, and a hot outlet equipped with a regulating valve to control the mass fractions. When a fluid is injected through the nozzles, a spinning vortex is generated inside the tube, where portion of the fluid leaves through the high temperature outlet and the other portion move back to leave through the cold temperature outlet. Although Ranque–Hilsch vortex tube (RHVT) has low thermal efficiency, it has a wide range of positive aspects, which make it attractive for many industrial applications. Vortex tube is a durable device since (1) it needs little maintenance as it has no moving parts, (2) it does not need special working fluid (Freon or other refrigerants), (3) it has light weight and (4) its outlet temperatures are easily adjustable.

Despite being used in various industrial applications [8, 23], the working mechanism of vortex tube is still contentious [27]. In 1933, Ranque [35] argued that the energy separation is due to the adiabatic expansion in the near axis region and adiabatic compression in the peripheral region. This idea has been adopted by Hilsch [26] in 1947, who also considered the viscous effect between fluid layers. However, the idea of fully adiabatic process has been later challenged by different research groups [3, 19, 22]. Fulton [19] has pointed that the friction between fluid's layers is the main reason of temperature separation. Before fluid flows away from the vortex generator, the structure of the flow consists mainly of a free vortex. In this region, friction allows the transfer of the kinetic energy, between the free and the forced vortex, in a higher rate than the transfer of heat. Consequently, the internal energy of the peripheral fluid will be higher than that of the near axis fluid. This argument has been supported by Gustol [22] who also states that the turbulent motion that are formed just at the outlet of the inlet nozzles cause mass transfer, which in turn leads to the exchange of kinetic and heat energy. Diessler [17] has claimed that turbulent mixing and turbulent shear work are the main reasons of the energy separation phenomenon. Gao [20] has claimed that these proposals cannot be fully accepted because those researchers used various turbulence parameters, which are difficult to be equal in all investigations, and they do not utilize the effect of geometrical parameters.

In 1990s, Ahlborn [1, 2, 4] proposed the secondary circulation model which refers the origin of energy transfer to the presence of two types of secondary circulation inside the tube, open and closed circulations. The open circulation is named the peripheral loop, and it passes from the inlet nozzles towards the hot orifice then move back to leave through the cold orifice. This loop can be divided into two portions, high temperature portion at the periphery of the tube and low temperature portion at the center of the tube. The closed circulation is named the secondary circulation loop, and it is enclosed by the peripheral loop. These two loops combined work operates as a refrigeration cycle where work is transferred from the peripheral to the near axis region and heat is transferred from the near axis region to the peripheral region. In this model, friction between fluid layers plays a crucial role where it decelerates the peripheral fluid adiabatically increasing its temperature [20]. Acoustic streaming is another proposed working mechanism of Ranque–Hilsch vortex tube [30]. It states that the acoustic wave generated by organized disturbances alters the free vortex to forced vortex, which leads to temperature separation [30]. Aljuwayhel et al. [5] explained that the vortex tube's energy separation is mainly due to work transfer mechanism which deteriorate as heat transfer between the cold and hot flow regions. The work transfer is prompted by the torque generated due to the viscous shear.

In literature, vortex tube design has received a lot of interest. The effect of wall insulation and nozzle configuration has been examined by [34]. It has been shown [21] that enhancing the formation of the vortex flow, in the core of VT, provides better energy separation performance. It has been reported [18] that optimum vortex tube performance is achieved when subsonic condition is adopted at the inlet nozzles.

When it comes to the assimilation of the energy separation phenomenon, it is beneficial to understand the significance of the working fluid in the vortex tube, which has been examined by different research groups [10, 25, 29, 31, 36–38]. Khazaei et al. [29] has studied the effect of utilizing various fluids on the radial temperature distribution. The results reveal that helium has the highest temperature gradient and carbon dioxide has the lowest one compared to nitrogen, air, oxygen, and ammonia. Moreover, it has

been shown [29] that air and nitrogen almost have the same radial temperature profile. As a result, it has been concluded that gases with higher specific heat and smaller molecular weight give the largest temperature difference. This conclusion matches the findings of Saidi et al. [36], who examined the energy separation using three gases, namely helium, oxygen, and air. On the contrary, Aydin et. al. [10] experimentally reported that nitrogen gave higher temperature difference, and this is attributed to the smaller molecular weight of nitrogen compared to oxygen and air. However, based on the values provided by Khazaei et al. [29], there is no substantial difference between them. It has been reported [25] that thermal diffusivity, kinematic viscosity and thermal conductivity are considered as main factors affect gas energy separation. The amount of energy separation depends on type of fluid used [38]. Liang [31] used numerical tool to investigate the coefficient of performance (COP) of a vortex tube working with binary gas mixture $CH_4 - CO_2$. It has been found that as the mole fraction of CH_4 increases, i.e. the molecular weight of the mixture decreases, the COP of the VT decreases. Also, Liang [31] reported that decreasing the amount of Methane in the mixture leads to an increase in the velocity and temperature separation. Vinceno Biano et al. [13]. investigated the energy separation phenomenon in VT using two different turbulence models, namely LES and RSM. The author reported that the LES model is more accurate than the RSM model, and that the turbulence very important effect of temperature different at the outlets of the tube. Alexandar et al. [28] used the entropy generation analysis to investigate the source of irreversibility in vortex tube. It was proposed that the optimization of VT should be done through altering the tube diameter, and the main nozzle geometry. Table. 1 shows some of the latest numerical investigation that has been done on vortex tube.

This study examines the effect of working fluid properties and viscosity heating on vortex tube performance. Many studies have examined different working fluid while referring the improvement or deterioration of performance to the value of these interrelations' properties. Therefore, to author's knowledge, this is the first attempt to investigate the impact of a single fluid property, independently from other properties, on the vortex tube performance. Moreover, it presents a detailed examination

of these fluid properties; namely, heat capacity, molecular weight, and thermal conductivity effects, on the flow and temperature fields. It is worth mentioning that pressure, temperature and density remain interrelated via the ideal gas equation of states. The ideal gas assumption hold for current study since operating pressure is much lower than the critical pressure and operating temperature is way higher than the critical temperature of the gas. In addition, altering a single property of the working fluid is not experimentally conceivable, though, this study has adopted this approach as a step towards understanding the impact of properties on energy separation in vortex tube. As stated in literature [5], the energy separation is driven by the work-transfer from the cold region to the hot region via vortex flow, while heat transfer from the hot region to the cold region inclines to reduce this energy separation.

2 Numerical modeling and formulation

To reduce the computational time, the numerical simulations are performed on a 90° sector of a real commercialized vortex tube model obtained from literature [24] for purpose of validation of this numerical study. The model is generated using a computational fluid dynamics (CFD) package ANSYS-fluent R19.1. Figure 1 and Table 1 demonstrate the geometric features of the modeled vortex tube. The energy separation effect in vortex tube could be reproduced by solving the fundamental conservative equations with the ideal gas law, which are listed below:

Conservation of mass

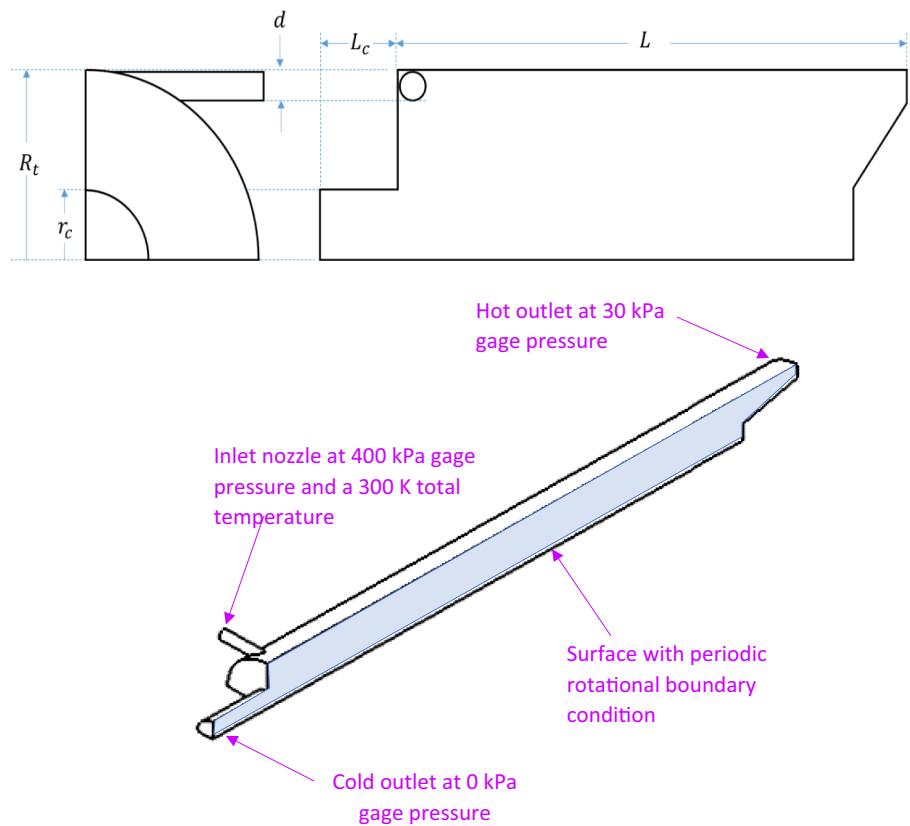$$\frac{\partial(\rho\bar{u}_i)}{\partial x_j} = 0 \tag{1}$$

Conservation of momentum

$$\frac{\partial\left(\rho\bar{u}_i\bar{u}_j\right)}{\partial x_j} = -\frac{\partial\bar{p}}{\partial x_i} + \frac{\partial}{\partial x_j}\left[\mu\left(\frac{\partial\bar{u}_i}{\partial x_j} + \frac{\partial\bar{u}_j}{\partial x_i}\right) - \rho\overline{u'_i u'_j}\right] \tag{2}$$

Conservation of energy

Table 1 Some numerical investigations on vortex tube

Author	Year	Investigation	References
Fachun Liang et. al	2022	Effect of hot end structure on energy seperation	[32]
James Cartlidge	2022	Performance of divergent vortex tube	[14]
Ahmad Alsaghir	2022	Sensitivity analysis of various design parameters	[7]
Adib Bazgir er. al	2019	Effect of cold tube fin geometry on thermal seperation	[12]
Adib Bazgir er. al	2018	Temperature separation in various VT models	[11]

Fig. 1 A two-dimensional schematic of the vortex tube with its main dimensions **a** side view, **b** front view and **c** isometric projection with boundary conditions

$$\frac{\partial\left(\rho\bar{u}_j\bar{T}\right)}{\partial x_j} = \frac{\partial}{\partial x_j}\left[\frac{\mu}{Pr}\left(\frac{\partial\bar{T}}{\partial x_j}\right) - \rho\overline{T'u'_j}\right] + \varphi \qquad (3)$$

Ideal gas law

$$\bar{p} = \rho R\bar{T} = \rho\left(R_u/MW\right)\bar{T}, \qquad (4)$$

where $\bar{u}$, $\bar{T}$, and $\bar{p}$ are the time-average velocity, temperature, and pressure, respectively. u'_j and T' are the instantaneous fluctuating velocity and temperature. Reynold's tensors in Eqs. 2 and 3 are modelled using Boussinesq approach as per the following equations (Eqs. 5, 6):

$$\rho\overline{u'_i u'_j} = \mu_t\left(\frac{\partial\bar{u}_i}{\partial x_j} + \frac{\partial\bar{u}_j}{\partial x_i}\right) - \frac{2}{3}\left(\rho k\delta_{ij} + \mu_t\frac{\partial\bar{u}_k}{\partial x_k}\right) \qquad (5)$$

$$\rho\overline{T'_i u'_j} = -\frac{\mu_t}{Pr_t}\left(\frac{\partial\bar{T}}{\partial x_j}\right), \qquad (6)$$

where μ_t, k and Pr_t are the turbulent viscosity, turbulent kinetic energy, and turbulent Prandtl number, respectively. The merit of this approach is the low computational cost associated with the calculation of μ_t. In this study the turbulent viscosity is computed in terms of the turbulent kinetic energy (k) and the specific dissipation rate (ω).

The SST $k-\omega$ turbulence model is used to model the turbulence flow. The SST $k-\omega$ turbulence model is a two-equation model where the turbulent viscosity is computed by utilizing the turbulent kinetic energy (k) and the specific dissipation rate (ω) as shown in the following equation:

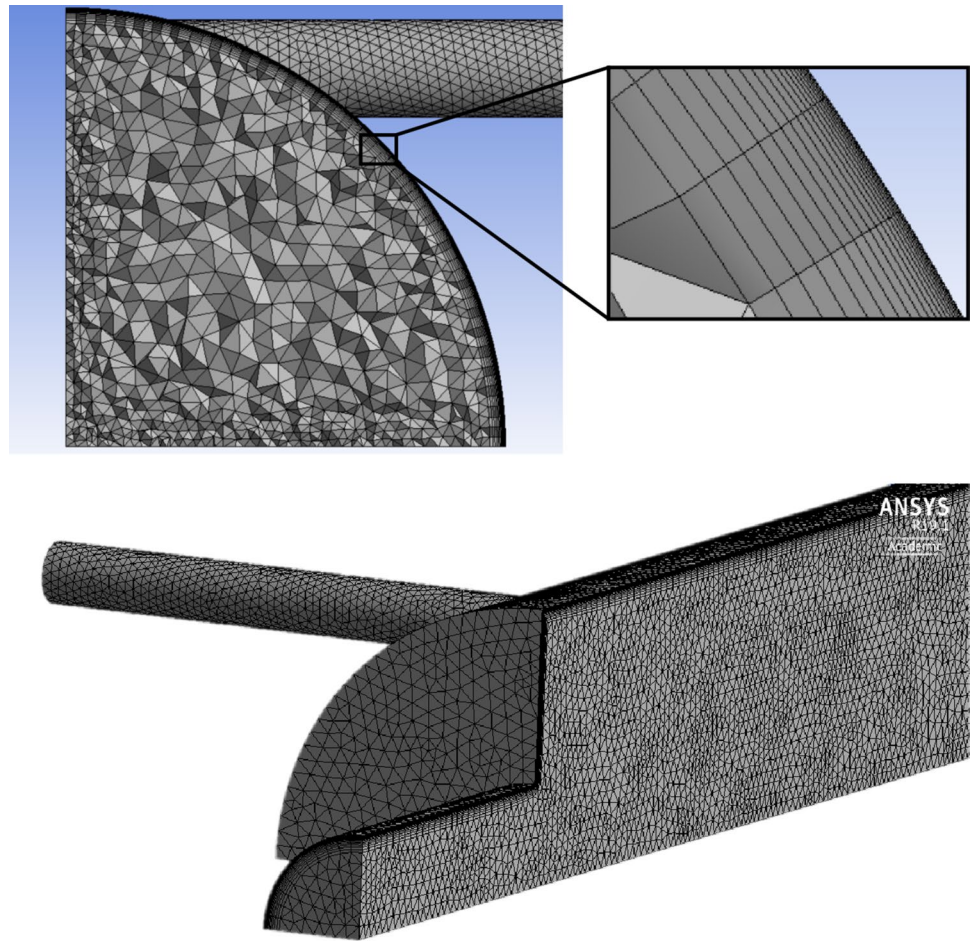$$\mu_t = \alpha^*\frac{\rho k}{\omega}, \qquad (7)$$

where α^* is a correction number used to damp the turbulent viscosity at low Reynold number. k and ω can be calculated using the following Eq. [9]:

Table 2 Dimensions of the vortex tube [24]

Parameter	Dimension (mm)
Tube radius (R_t)	7.24
Tube length (L)	97.00
Cold outlet length (L_c)	10.00
Cold outlet radius (r_c)	2.72
Nozzle diameter (d)	1.60

Fig. 2 Unstructured mesh of the modeled vortex tube with maximum element size of 0.4 mm and wall inflation layer. The magnified zone near the wall shows a starting element of thickness of 0.0035 mm with inflation layer growth rate of 1.2

$$\frac{\partial}{\partial t}(\rho k) + \frac{\partial}{\partial x_i}\left(\rho k \overline{u_i}\right) = \frac{\partial}{\partial x_i}\left(\Gamma_k \frac{\partial k}{\partial x_j}\right) + G_k - Y_k + S_k \quad (8)$$

$$\frac{\partial}{\partial t}(\rho \omega) + \frac{\partial}{\partial x_i}\left(\rho \omega \overline{u_i}\right) = \frac{\partial}{\partial x_j}\left(\Gamma_\omega \frac{\partial \omega}{\partial x_j}\right) + G_\omega - Y_\omega + D_\omega + S_\omega \quad (9)$$

More detail regarding the variables shown in Eqs. (8) and (9) are explained in ANSYS user guide [9].

The equations above are solved numerically under the assumption of steady state where thermal conductivity, heat capacity and dynamic viscosity are assumed constant. This assumption is acceptable since the expected temperature change is less than 35 °C. This assumption is adopted to allow studying the effect of varying these properties with large difference. The viscous heating is examined in this study since Brinkman number (Br) is of order 1. As reported in literature [33], viscous heating occurs because of high tangential velocity near the vortex tube peripheral.

2.1 Physical setup and boundary conditions

Steady, pressure-based solver is utilized to simulate the energy separation phenomenon in the VT. In the solution method the coupled scheme is used with third order discretization in density, momentum, energy, turbulent kinetic energy, and specific dissipation rate equations. Five different gases, namely, air, oxygen, nitrogen, carbon dioxide and helium are examined. Table 2 shows the default properties of these gases that are provided by ANSYS CFD tool. Air is chosen to be the control gas, and its default properties are used to nondimensionalize the independent variable properties. The residuals are set to 10^{-9} for energy and to 10^{-6} for continuity, velocity, k, and ω. The physical boundary conditions that are used in this study are as follow:

a. Rotational periodic boundary conditions about the axis of the tube.
b. A 400kPa gage pressure and a total 300K as inlet boundary conditions.
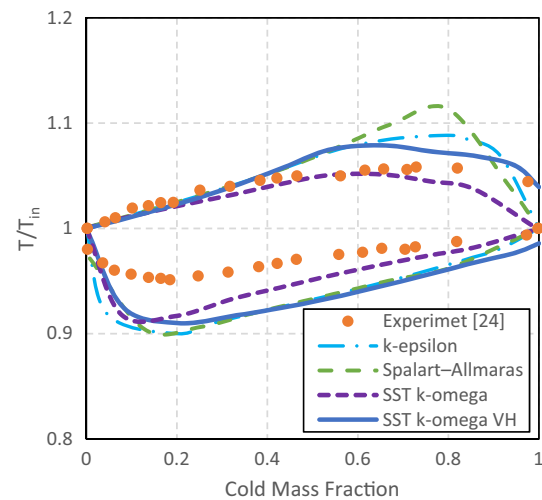c. A 30kPa gage pressure as outlet boundary condition at the hot end.

(a)

(b)
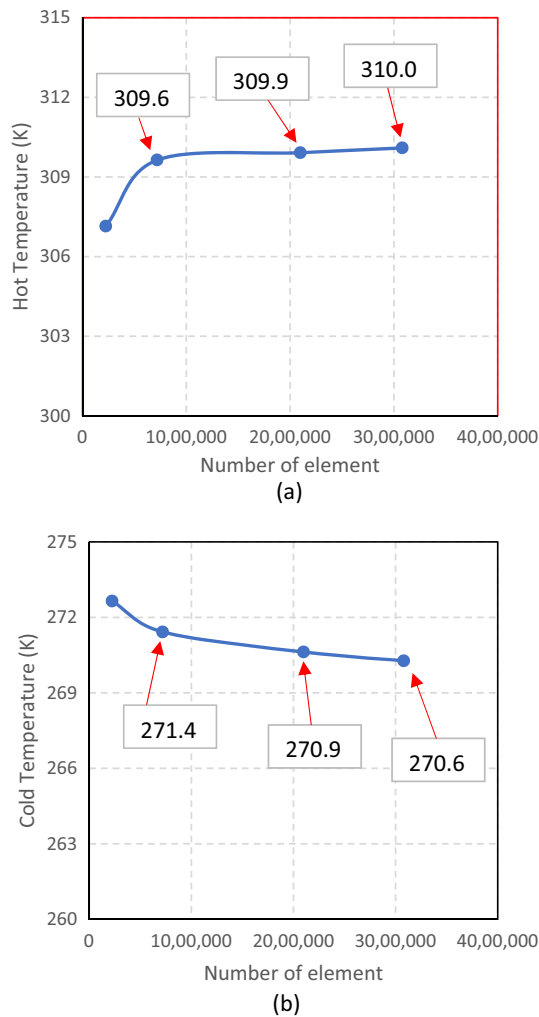
**Fig. 3** Effect of number of elements on **a** the hot and **b** the cold outlet temperatures

Fig. 4 Validating the of different turbulence numerical models with the experimental data in [24] by plotting outlet total temperature ratio from numerical study and experiment recovery temperature with respect to mass fraction (temperature ratio greater than one is for hot outlet and temperature ratio less than is for cold outlet)

y^+ is maintained around 1, which is achieved by setting the first element near the wall with size of 0.0035 mm. An inflation layer with growth rate of 1.2 is applied at the tube walls. To make sure that the obtained results are independent of number of nodes within the grid, a mesh independent study is done based on the observation of the facet maximum hot outlet temperature and facet minimum cold total temperature, as shown in Fig. 3. It is clear that at 720,175 elements, which corresponds to 0.4 mm element size, the effect of element size becomes trivial, which indicates that the mesh independence is achieved at this size.

d. A $0 kPa$ gage pressure as outlet boundary condition at the cold end.
e. An adiabatic with no slip boundary condition at the walls of the tube.

In part of the study, the impact of mass fraction has been examined by varying the pressure outlet value. Otherwise, a fixed value of $30 kPa$ gage pressure is used as stated earlier. Also, to allow examining velocity and temperature variation in radial velocity, a fix location of $z/L = 0.63$ have been selected which is represent the middle region of the VT.

2.2 Mesh independence

Figure 2 shows the unstructured mesh that is used in this research. To correctly capture the viscous sublayer, the wall

3 Results and discussion

Dimensionless parameters are used to demonstrate the results of the numerical simulation. The total pressure of $P_{in} = 400 kPa$, the total temperature of $T_{in} = 300K$ and the inlet velocity of air are used to produce the dimensionless parameters. All profiles are obtained at dimensionless z-axis distance of $z/L = 0.63$. Most of these profiles depict the fact that the flow structure inside vortex tube consists of two vortices. The first one is the forced vortex where velocity increase with radius. The second one is the free vortex where velocity decrease with radius. This finding matches with [6] who showed the detailed velocity profile of each vortex. Regarding the physical properties, they are nondimensionalized based on the values of air properties provided in Table 2. The numerical results are validated by reproducing the published experimental data [24],
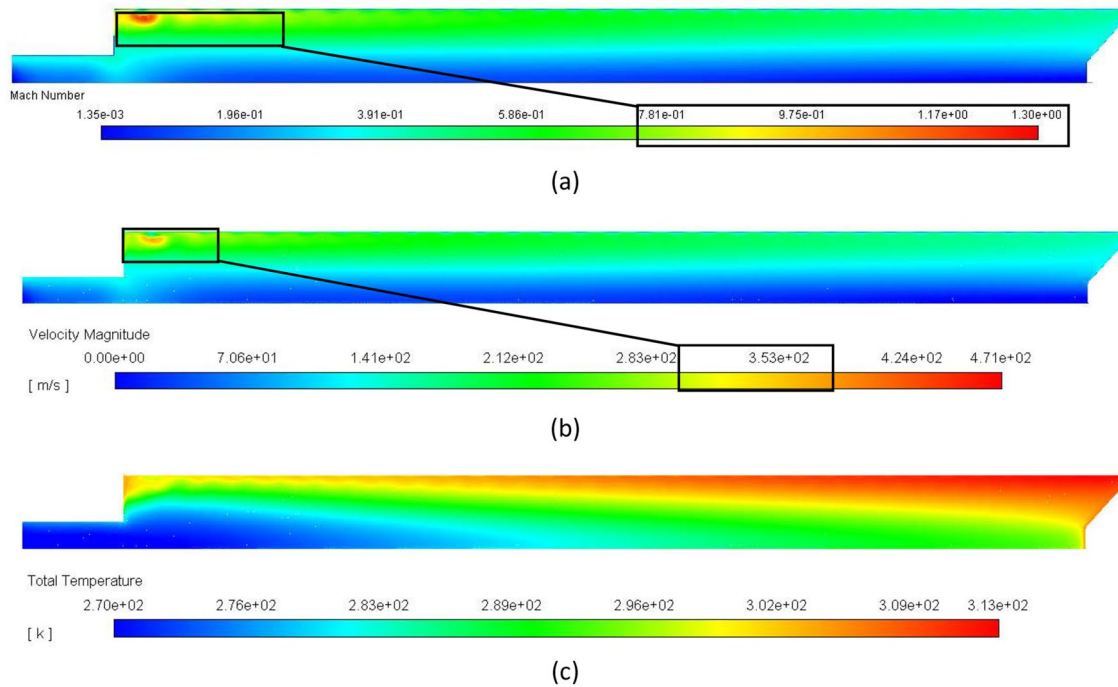
Fig. 5 Contour plots at the period surface for air **a** Mach number contour, **b** velocity magnitude, **c** total Temperature
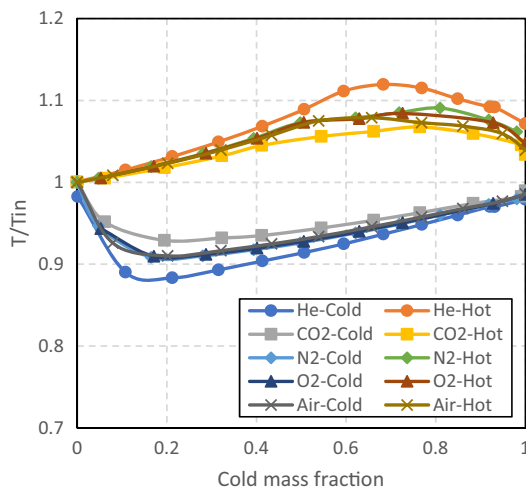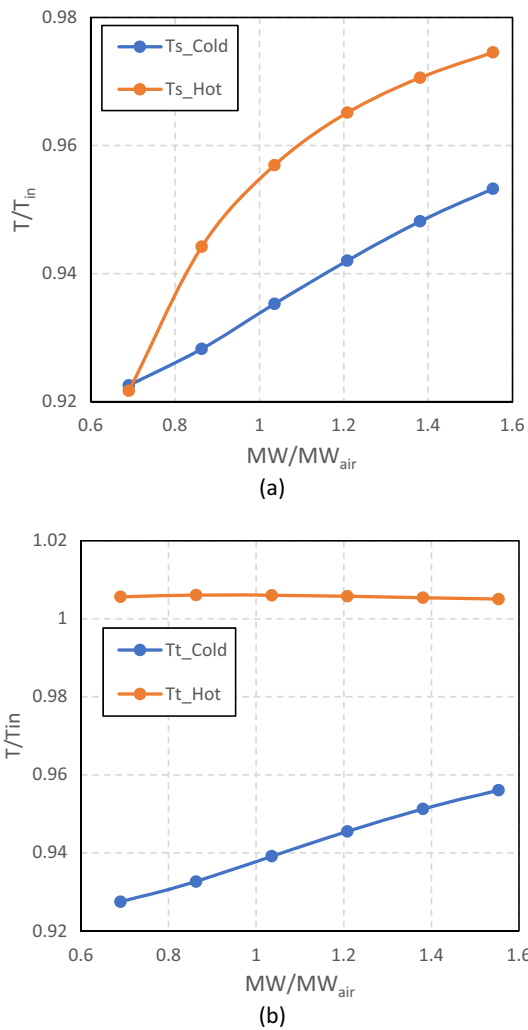

Fig. 6 Effect of cold mass fraction on the dimensionless total outlet temperature for different gases with 400 kPa at the inlet, 0 kPa at the cold outlet and variable pressure at the hot

as shown in Fig. 4. Figure 4 shows that the three turbulence models, namely Spallart-model, $k - \varepsilon$, and between $SSTk-\omega$, are capable of predicting the energy separation phenomenon. However, it can be noticed that the $SSTk-\omega$ is most appropriate as it shows better matching with the experimental results, especially at high cold mass fraction. When viscous heating is enabled, $SSTk-\omega VH$, the model is capable to predict the temperature separation that has

been reported during experiment [24], mainly around mass fraction of 1. Hence, viscous heating is adopted for the rest of the study. All the CFD models over predicting the experimental findings since the CFD is reporting the total mass weighted average temperature while the experimental study reports the recovery temperature. Hence, the recovery (actual) temperature will be less.

The contours plots for Mach number, flow velocity and temperature are shown in Fig. 5. It is clear that viscous heating phenomenon mainly acts in the vortex generator region because this is the only region where Mach number exceeds 1, as shown in Fig. 5a. Figure 5b shows that the velocity magnitude increases in the radial direction where it reaches its maximum values in the near wall region. This variation controls the change of total temperature inside the vortex tube as it reaches maximum in the same region, Fig. 5c.
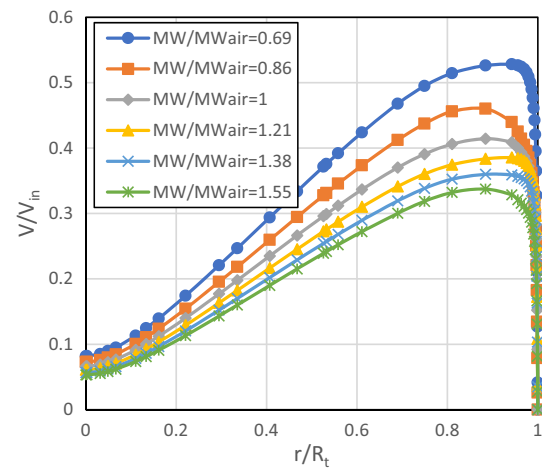
Figure 6 depicts the influence of the cold mass fraction, which is the ratio of the cold outlet mass flow rate to the inlet mass flow rate, on the energy separation in a vortex tube operating with different gases. As it has been shown in the experimental study with air [24], the relationship between the outlets temperatures and the mass fractions is non-monotonic, and the optimum hot and cold temperatures occur at different mass fractions. Moreover, it is clear that the best temperature separation is achieved by helium, which has the highest heat capacity (HC) and the lowest molecular weight (MW). On the other hand, carbon

(a)

(b)

Fig. 7 Effect of molecular weight ratios on dimensionless **a** static and **b** total outlet temperatures with 400 kPa at the inlet, 0 kPa at the cold outlet and 30 kPa at the hot outlet

Fig. 8 Dimensionless velocity profiles versus dimensionless radial direction plotted at $z/L = 0.63$ for various molecular weight ratios with 400 kPa at the inlet, 0 kPa at the cold outlet and 30 kPa at the hot outlet
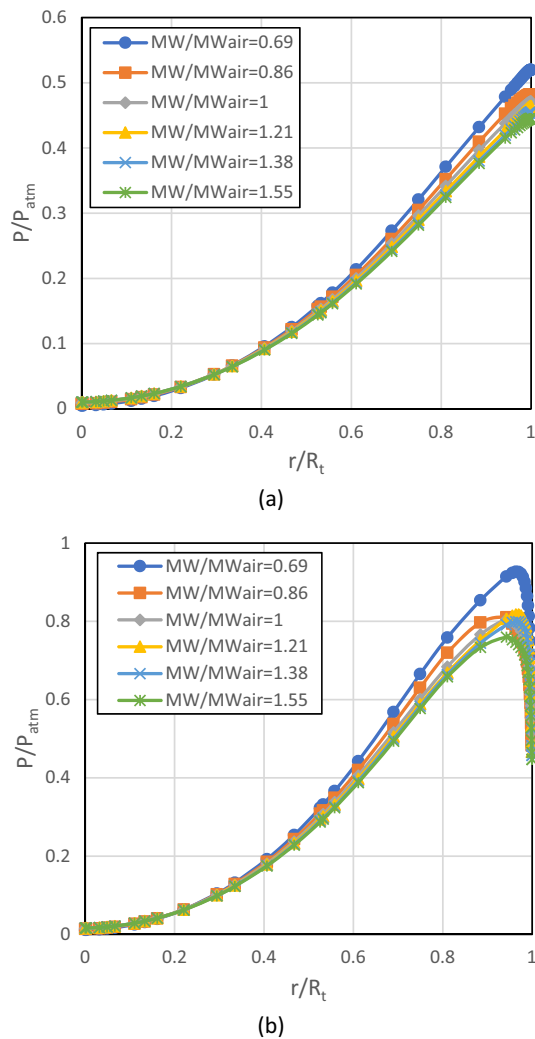
as shown in Figs. 7, 8, 9, 10, 11, 12, 13, 14, 15, 16, 17, 18, 19, 20, and 21. These figures are produced using air as working fluid while altering one fluid property at a time. Such alteration of a single property is not achievable experimentally without impacting other fluid properties. Such study is easily done numerically and offers great benefit to understand the energy separation behavior of different fluids.

The impacts of MW on flow fields are shown in Figs. 7–11. Figure 7 illustrates the impact of MW of a gas on the outlet temperatures. Overall, it can be seen that the MW can significantly affect the static temperatures, Fig. 7a, and the cold total temperature, Fig. 7b, while it approximately has no minute effect on the hot total temperature, Fig. 7b. Furthermore, increasing the MW leads to a substantial increase in the values of both the static and total temperatures of the cold outlet. For given VT design conditions, when the molecular weight ratio increases from 0.69 to 1.55, both the static and total cold temperature ratios increase from 0.92 to 0.95, which correspond to 9 °C rise in the temperature of the cold fluid. Although the effect of increasing MW has improved the hot static temperature, about 8.7 °C, it shows a minor decrement in the hot total temperature. To properly explain the impact on static and total temperature, one needs to refer to the relation between these temperatures in Eq. (10)[15],

$$T_t = T_s + \frac{V^2}{2C_p} \qquad (10)$$

The equation above clearly shows that total temperature is significantly larger than the static temperature at high velocities, which is observed at the hot outlet. It also

dioxide with the lowest HC and the highest MW yields the lowest energy separation performance, which agree with published numerical results [29]. When the vortex tube is modeled with air, nitrogen, or oxygen, the simulations have shown that these gases behave in a similar way and no significant difference in outlet temperature has been observed. One can attribute this to the fact that these gases have similar HC and MW. Figure 6 results show that the performance of energy separation depends on many properties such as molecular weight, thermal conductivity, heat capacity and dynamics viscosity. In order to properly investigate the impact of each property, a numerical simulation is performed varying only one property while fixing the rest of the properties as show in next sections.

As mentioned earlier, the benefit of using CFD analysis that it allows isolating the effect of single fluid property from other properties as well as it offers details of the flow,
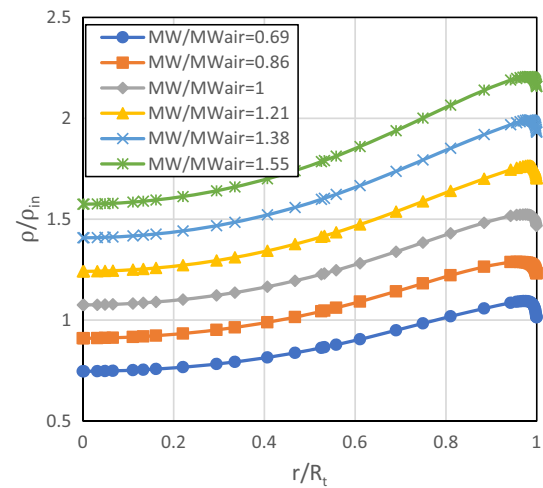
(a)

(b)

Fig. 9 Dimensionless pressure profiles versus radial direction plotted at $z/L = 0.63$ for various molecular weight ratios. **a** Static and **b** total pressures with 400 kPa at the inlet, 0 kPa at the cold outlet and 30 kPa at the hot outlet
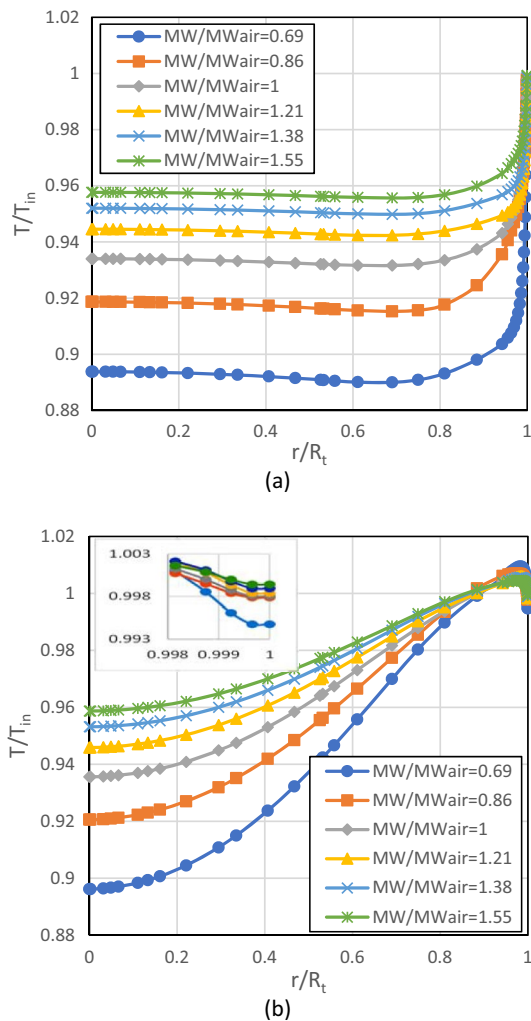

Fig. 10 Dimensionless density profiles versus dimensionless radial direction plotted at $z/L = 0.63$ for various molecular weight ratios with 400 kPa at the inlet, 0 kPa at the cold outlet and 30 kPa at the hot outlet

indicates that the total temperature approaches to the static temperature at low velocities, which is observed at the cold outlet.

The expected high velocities at the hot outlet and low velocities at the cold outlet can be clearly seen in Fig. 8. Based on the VT structure, the hot gas leaves near the tube periphery while the cold gas leaves near the center of the tube. As show in Fig. 8, the velocity magnitude is high near the tube periphery, and low near the center. The periphery experiences high velocities, while the tube center region experiences low velocities due to the tangential nozzle arrangement that cause a strong vortex formation in the VT. It is more difficult to move heavy particles (high MW) compared to light weight particles (low MW). Hence, due to the concept of momentum conservation, as expected high MW particles have lower velocities compared to the

low MW particles, as show in Fig. 8. Also, for selected axial location $z/L = 0.63$, it is clear that forced vortex is formed for $0 < r/R_t < 0.9$, which get slowdowns near the tube periphery due to no-slip condition and boundary layer formation. Since the main focus of this work is to examine the behavior of energy separation for different gases, the study examined only one axial location (z/L). The flow behavior at different axial locations has been examined in different places in literature [6]. In more details, the impact of the MW is clearly observed from ideal gas equation in Eq. (4), which shows that MW is directly proportional to static temperature and density while inversely proportional to the static pressure. At a specific axial location of $z/L = 0.63$, the impact of MW on pressure, density and temperature are shown in Figs. 9, 10 and 11, respectively. The impact of MW on static and total dimensionless pressure profiles at a fixed axial location of $z/L = 0.63$ is shown in Fig. 9. Figure 9a shows the dimensionless static pressure profile in radial direct for different MW ratios. For a fixed MW, Fig. 9a shows that the dimensionless static pressure increases in radial direction due to the centrifugal force produced by the vortex flow that pushes the gas particles toward the tube. Moreover, it is clear that the dimensionless static pressure decreases at larger MWs, which agrees with the ideal gas law shown in Eq. (4). In Fig. 9b, the dimensionless total pressure increases radially until starts decreasing about the tube periphery. This pressure profile is due to the fact that the total pressure depends on static pressure and fluid velocity as in Eq. (11). While static pressure increases radially, velocity increases then decreases due to the no-slip condition near the periphery. Also, the total pressure decreases as MW increases, which
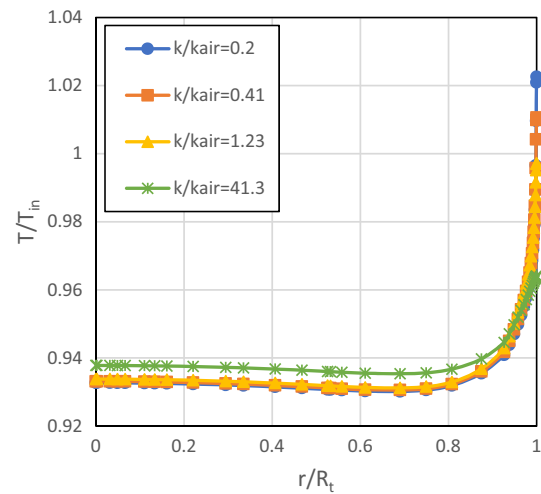
(a)

(b)

Fig. 11 Dimensionless temperature profiles versus dimensionless radial direction plotted at $z/L = 0.63$ for various molecular weight ratios. **a**) Static and **b** total temperatures with 400 kPa at the inlet, 0 kPa at the cold outlet and 30 kPa at the hot outlet

is expected since as MW increases, both the static pressure and the velocity magnitude decrease.

$$P_t = P_s + \frac{1}{2}\rho V^2 \quad (11)$$

Figure 10 shows that density increases in radial direction due to the vortex centrifugal force, which pushes more particles near the tube periphery. An increase in number of particles leads to an increase in gas density. The figure also shows that density is proportional to MW that is expected as shown in Eq. (4).

Figure 11a shows the dimensionless static temperature profile in radial direction at a specific axial location of $z/L = 0.63$ for different MW ratios. The figure shows that the dimensionless static temperature decreases in radial direction and then increases toward the tube periphery.

Fig. 12 Dimensionless static temperature profiles versus dimensionless radial direction plotted at $z/L = 0.63$ for various thermal conductivity ratios with 400 kPa at the inlet, 0 kPa at the cold outlet and 30 kPa at the hot outlet

This profile is dictated by the static pressure and density, which are shaped by the vortex flow centrifugal force. By examining Eq. (4), $\overline{T} = \overline{p}/(\rho R)$ with Figs. 9 and 10, it is clear that static pressure ($\overline{p}$) increases in radial direction while the inverse density ($1/\rho$) decreases, hence a non-monotonic relation for static temperature is expected. These relations yield high static temperature values at the center of the tube and the walls while low in between. The figure also shows that an increase in MW causes a rise in the static temperature for the entire radial axis. It was formulated in the ideal gas equation and confirmed from the figure that the static temperature is directly proportional to MW. On the other hand, in Fig. 11b, the increase in MW causes a rise in the total temperature within the forced vortex ($0 < r/R_t < 0.75$). However, outside the forced vortex, predicting the trend is inconsistent. Nonetheless, with proper zooming in Fig. 1b close-up, the same trend is observed near the wall as well. The figure also illustrates that the coldest static temperature occurs inside the tube at any MW ratio, which indicates a heat transfer from the center and the wall of the VT to the coldest point region.

The impacts of thermal conductivity (TC) on temperature separation are shown in Table 3 and Fig. 12. As shown in Table 3, a TC value of $k_f = 1$ W/m K is tested which shows that thermal conductivity has no impact on energy separation. The value of $k_f = 1$ W/m K is considered a high value for gaseous fluid. In general, increasing the TC has no effect on the temperature of outlet streams. It can be seen that as the TC increases from 0.005 W/m K to 0.04 W/m K the change in temperature is less than 1 Kelvin. The same trend is observed in Fig. 12 that shows the static temperature profile in radial direction at $z/L = 0.63$.

(a)

(b)
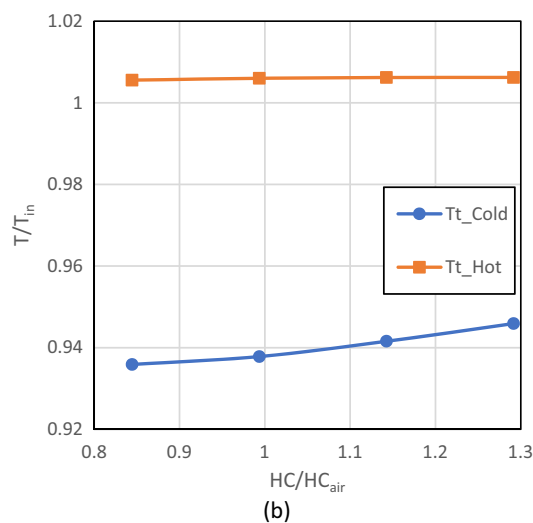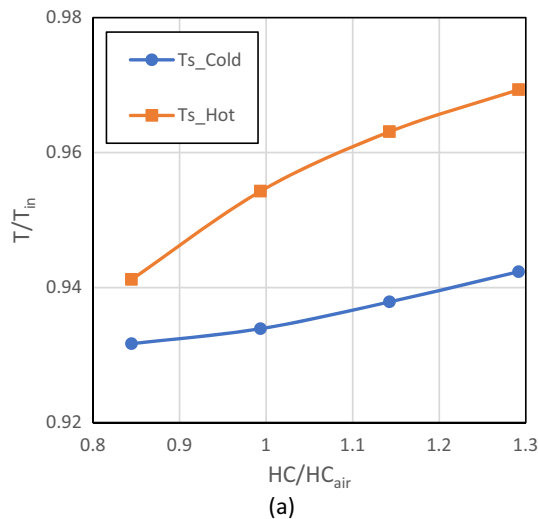
Fig. 13 Effect of heat capacity ratios on dimensionless **a** static and **b** total outlet temperatures with 400 kPa at the inlet, 0 kPa at the cold outlet and 30 kPa at the hot outlet

It is clear that the static temperature profile does not significantly change with variation of TC. The temperature profile indicates that small amount of heat transfers from the VT wall and center to the coldest point in the profile. This static temperature profile does not depend on the TC ratios. It depends on the static pressure and density, which are independent from the TC ratios. This conclude that the heat transfer in radial direction is insignificant and does not justify the energy separation in the vortex tube (Table 4).

The impacts of heat capacity (HC) on flow fields are shown in Figs. 13–16. Figure 13 presents the variation of outlet temperature of the VT as a function of HC. Although, the incremental change of the HC causes an increase in the static and the cold total temperatures, it shows a plateau effect on the hot total temperature. For a moment,
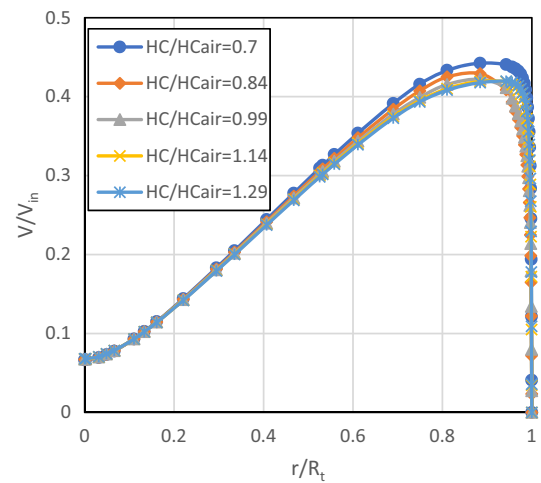
Fig. 14 Dimensionless velocity profiles versus dimensionless radial direction plotted at $z/L = 0.63$ for various heat capacity ratios with 400 kPa at the inlet, 0 kPa at the cold outlet and 30 kPa at the hot outlet

noticing the impact of HC on the energy separation could sound confusing, since it is well-known that in steady state operation (like VT operation), the HC does not affect temperature distribution [16]. The HC has no effect on energy separation but it impacts amount of energy entering with the flow as $h = c_p T$. The energy entering with the mass flow rate is getting distributed due to the vortex flow structure, hence, HC increase cause an increase in the static temperature as shown in Fig. 13a. From Fig. 13b and Eq. (10), the cold total temperature is directly proportional to the cold static temperature since the cold outlet velocity is small. However, the hot total temperature showed a plateau relation with HC since its value is dominated by the velocity value at the hot outlet. The hot outlet velocity is very high (near sonic) that explains no effect of HC on the hot total temperature. At specific axial location of $z/L = 0.63$, the impact of HC on temperature and pressure are shown in Figs. 14 and 15, respectively. The effect of HC on the fluid velocity profile at a specific axial location ($z/L = 0.63$) is shown in Fig. 14. It is clear from the figure that HC has a minor effect on velocity. Nevertheless, as HC increases the velocity decreases. This behavior is due to the fact that the particles with low HC have less ability to store the thermal energy as their internal energy. Hence, this energy is transformed as an increase in the kinetic energy of particles leading to an increase in their velocity.

The impact of HC on pressure is shown in Fig. 15. As shown in Fig. 15a, the static pressure decreases as HC increases, which is in agreement with the velocity magnitude results in Fig. 14. Because the drop in velocity causes a drop in the centrifugal force that leads to a drop in the static pressure. From Fig. 15b, the total pressure decreases
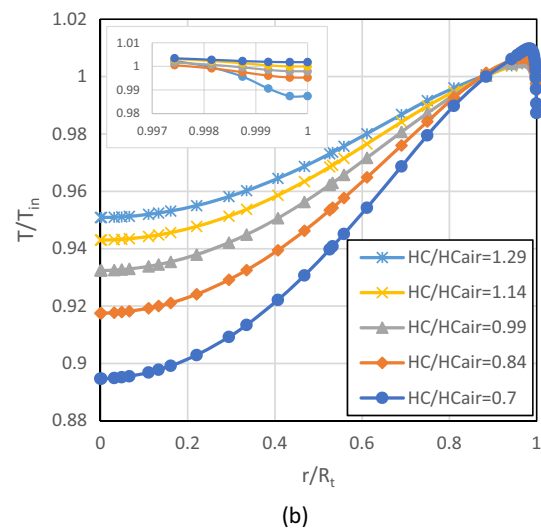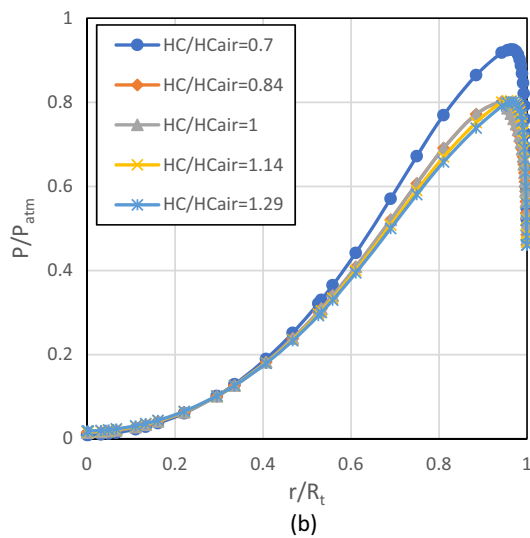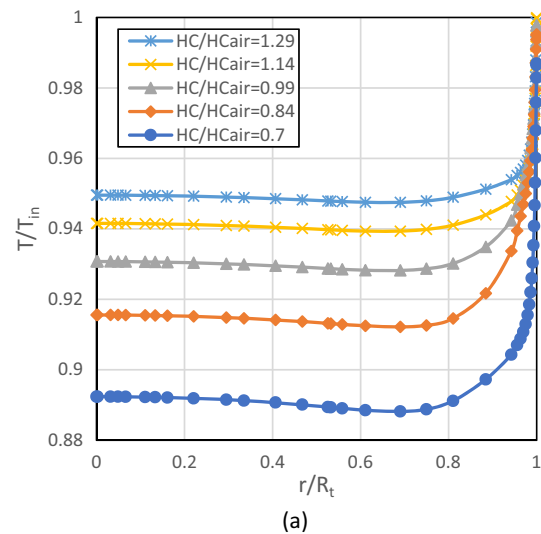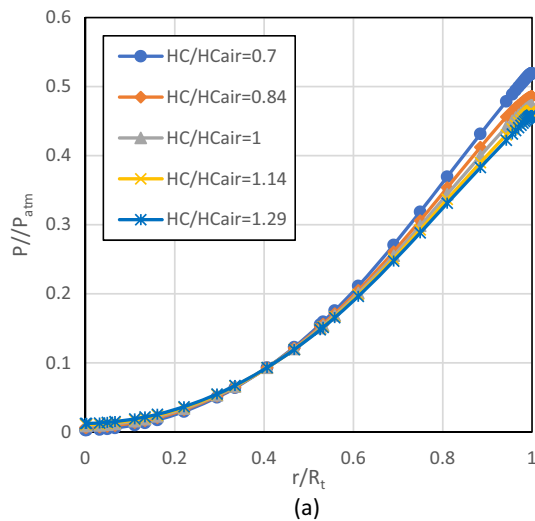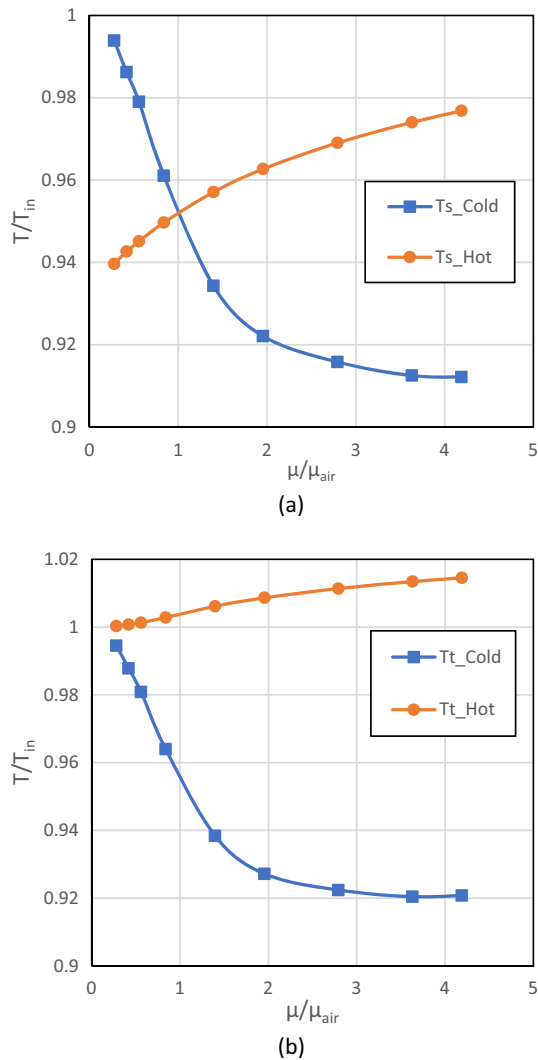
Fig. 15 Dimensionless pressure profiles versus dimensionless radial direction plotted at $z/L = 0.63$ for various heat capacity ratios. **a** Static and **b** total pressures with 400 kPa at the inlet, 0 kPa at the cold outlet and 30 kPa at the hot outlet

Fig. 16 Dimensionless temperature profiles versus dimensionless radial direction plotted at $z/L = 0.63$ for various heat capacity ratios. **a** Static and **b** total temperatures with 400 kPa at the inlet, 0 kPa at the cold outlet and 30 kPa at the hot outlet

as HC increases. The total pressure behavior is expected, as per Eq. 11, which indicates that both the static pressure and the velocity magnitude decrease at higher HC.
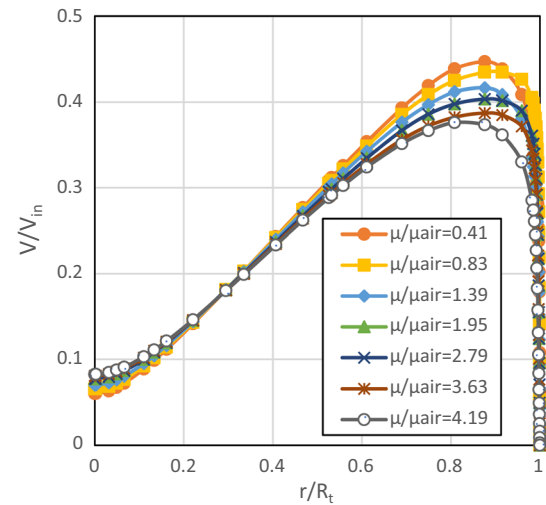
Figure 16 presents variation of dimensionless temperature profile versus radial axis at a specific axial location of ($z/L = 0.63$) for different HC ratios. From Fig. 16a, it is clear that the increase in HC rises the static temperatures inside the tube. The rise in the static temperature is due to the

increase in the total energy of the gas injected inside the VT. The increase in HC allows more energy to enter the VT tube, which leads to higher static temperatures. For total dimensionless temperature profile in Fig. 16b, the increase in HC causes a rise in the total temperature, which can clearly be seen in the force vortex region of $0 < r/R_t < 0.9$. With a proper zooming near the wall, as shown in the close-up of Fig. 16b, the same trend of forced vortex is observed near the wall too.

(a)

(b)

Fig. 17 Effect of dynamic viscosity ratios on dimensionless **a** Static and **b** total outlet temperatures with 400 kPa at the inlet, 0 kPa at the cold outlet and 30 kPa at the hot outlet
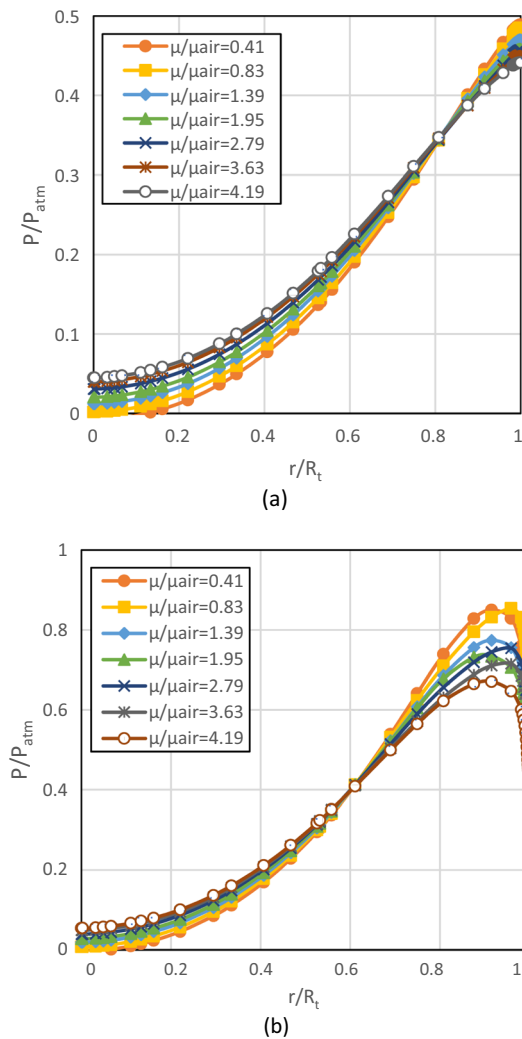

Fig. 18 Dimensionless velocity profiles versus dimensionless radial direction plotted at $z/L = 0.63$ for various viscosity ratios with 400 kPa at the inlet, 0 kPa at the cold outlet and 30 kPa at the hot *outlet*

This could be another justification on why helium, which has the highest viscosity as shown in Table 2, gives the best temperature separation performance.

To properly understand the impact of DV on energy separation, the velocity, pressure, density, and temperature profiles that are examined in Figs. 18, 19, 20 and 21, respectively. Figure 18 shows that the dimensionless velocity magnitude increases radially until a maximum value, then decreases until no-slip condition at the tube wall. The figure also shows that as dynamic viscosity ratio increases, the viscous forces diffuse toward the tube center. Hence, as DV ratio increases, the maximum velocity decreases while velocity at the center region increases.

Figure 19 shows that as DV increases, the dimensionless pressure increases near the center while decreases near the periphery. This effect occurs due to the angular momentum transfer from periphery to the tube center region. The pressure difference in radial direction decreases as DV increases. This angular momentum transfer reduces the centrifugal forces and hence reduce the pressure difference in radial direction. As shown in Fig. 20, density follow similar behavior as total pressure. This behavior of density is expected since higher density particles is pushed toward the periphery while lower density particle is accumulated near the center. Near the wall of tube, the velocity drops due to no-slip condition and hence density drop again.

Figure 21a shows the dimensionless static temperature profile in radial direction for different DV ratios. The dimensionless static temperature decreases slightly in radial direction until a minimum value of around $r/R_t = 0.75$., after which it starts increasing toward the tube periphery.

The impacts of dynamic viscosity (DV) on flow fields are shown in Figs. 17–21. Figure exhibits the impact of the dynamic viscosity on the VT outlet temperatures. The figure shows that increasing DV increases temperature difference between cold and hot outlets (i.e., improves energy separation). As the DV increases, the hot outlet temperatures (static and total) increase, while the cold side decrease. More specifically, when the DV ratio increases from 0.3 to 4.3, the hot end witnesses sharp increase in the static temperature, $\Delta T \cong 12\,°C$, and mild increase in the total temperature, $\Delta T \cong 4\,°C$. Also, both the static and the total cold temperatures substantially decrease with the increase in DV, until it reaches $\mu/\mu_{air} = 3.5$. Beyond DV ratio of 3.5, the change in outlet temperatures is minute and could be neglected. The temperatures of the cold stream drop about 23 °C between $\mu/\mu_{air} = 0.3$ and $\mu/\mu_{air} = 3.5$.
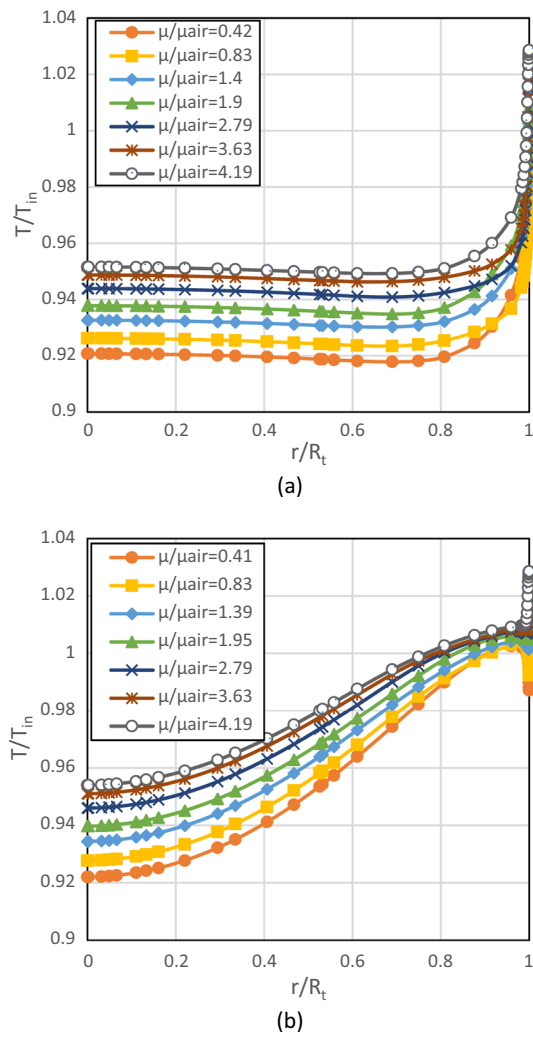
Fig. 20 Dimensionless density profiles versus dimensionless radial direction plotted at $z/L = 0.63$ for various dynamic viscosity ratios with 400 kPa at the inlet, 0 kPa at the cold outlet and 30 kPa at the hot outlet

Fig. 19 Dimensionless pressure profiles versus dimensionless radial direction plotted at $z/L = 0.63$ for various dynamic viscosity ratios. **a** Static and **b** total pressures with 400 kPa at the inlet, 0 kPa at the cold outlet and 30 kPa at the hot outlet

The shape of this profile is dictated by the static pressure and density, which are shaped by the vortex flow centrifugal force. By examining Eq. (4), $\overline{T} = \overline{p}/(\rho R)$, it is clear from Figs. 19 and 20 that in radial direction the static pressure ($\overline{p}$) increases while the density inverse ($1/\rho$) decreases. Therefore, a non-monotonic relation for static temperature is expected, which yields high values at the walls and the center while low values in between. The figure also illustrates that the rise in DV increases the difference between the minimum and the maximum temperatures in the static temperature profile. Figure 21 reveals that as the viscosity of the working gas increases, both static and total temperatures increase inside the tube. Moreover, the magnitude of the static temperatures at the wall increases
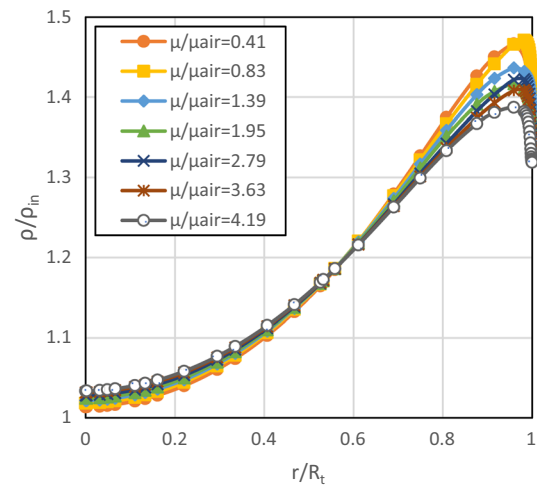
with viscosity and reaches a slightly higher value than the near axis temperature. From the total temperature profile in Fig. 21b, escalating the value of dynamic viscosity rises the total temperature along the radius of the tube. Moreover, as long as the dynamic viscosity ratio is less than 1.95, the temperature profile follows the same trend as the velocity profile, which decreases near the wall.

It worth to mention, that in general turbulent viscosity in the turbulent region is much higher than the molecular DV, hence its impact on viscous heating is more pronounced. As stated earlier, this work focuses on the impact of DV which has notable impact on the energy separation, as shown in Figs. 17–21. The reason of such impact appears in the low velocity region where DV contribute to kinetic energy transfer (work) from periphery flow region to core region. A high DV values mean a high shear force between rotating fluid layer which improve the work transfer in radial direction, hence improving the energy separation.

4 Conclusions

The numerical simulation has been verified by comparing the results with experimental data for wide range of cold mass fractions. The results reveal that helium yields the maximum separation while carbon dioxide the lowest. Air, nitrogen, and oxygen show a similar moderate

(a)

(b)

Fig. 21 Dimensionless temperature profiles versus dimensionless radial direction plotted at $z/L = 0.63$ for various dynamic viscosity ratios. **a** Static and **b** Total temperatures with 400 kPa at the inlet, 0 kPa at the cold outlet and 30 kPa at the hot outlet

temperatures are examined and the results indicate the following,

- The SST $k - \omega$ turbulence model with a proper wall condition ($y + < 5$) shows an acceptable capability to predict the experimental data.
- Viscous dissipation needs to be considered when modeling vortex tube and its impact mainly appears at the vortex generation region.
- The vortex tube energy separation increases as the molecular weight and the heat capacity decrease, while the dynamic viscosity increases.
- Increasing the molecular weight or the heat capacity of the working fluid decreases velocity, static pressure, and total pressures in the peripheral region of the tube only. Similarly, increasing the dynamic viscosity decreases the velocity and pressures in the peripheral region, while increases them in the near axis region.
- Varying the thermal conductivity shows no impact on the temperature inside the tube or at the outlets. Hence, the heat transfer in radial direction cannot be used to justify the energy separation in the vortex tube.
- At a fixed axial location, the static temperature decreases radially until a minimum value, then it increases radially toward the tube periphery. The sudden increase in the near wall region refers to the steep velocity gradient in this region which increase the effect of viscous shear in that region and consequently, the viscous hear generation.
- The dynamic viscosity of the fluid plays a crucial role in energy separation in the vortex tube as long as $\mu/\mu_{air} < 3.5$, since it allows greater static temperature along the radial direction. The dynamics viscosity effect supports the idea that work-transfer theory causes the energy separation between the periphery stream and the core flow.

temperature separation. Furthermore, the effect of gas properties such as molecular weight, heat capacity, thermal conductivity and dynamic viscosity on the outlet

Table 3 Thermo-physical properties of the tested gases

Gas	Molecular weight (kg/kmol)	Heat capacity (J/kg K)	Dynamic viscosity (kg/m s)	Thermal conductivity (W/m K)	Gas constant (J/kg K)
Air	28.966	1006.43	1.7894e−05	0.0242	287
Oxygen	31.9988	919.31	1.919e−05	0.0246	260
Nitrogen	28.0134	1040.67	1.663e−05	0.0242	297
Helium	4.0026	5193	1.99e−05	0.152	208
Carbon dioxide	44.00995	840.37	1.37e−05	0.0145	189

Table 4 Effect of thermal conductivity on outlet temperatures

k_f (W/m K)	k_f/k_{air} (–)	$T_{s.Cold}$(K)	$T_{s.Hot}$(K)	$T_{t.Cold}$(K)	$T_{t.Hot}$(K)
0.005	0.207	279.379	286.7418	280.66	301.975
0.01	0.413	278.9891	286.861	280.2953	302.04
0.02	0.826	278.6455	286.9721	279.9728	302.101
0.03	1.24	278.4154	287.0432	279.7557	302.141
0.04	1.653	278.2434	287.0971	279.5931	302.171
1	41.32	276.3433	287.7653	277.7672	302.557

Declarations

References

1. Ahlborn BK, Gordon JM (2000) The vortex tube as a classic thermodynamic refrigeration cycle. J Appl Phys 88:3645–3653
2. Ahlborn B, Groves S (1997) Secondary flow in a vortex tube. Fluid Dyn Res 21:73
3. Ahlborn B, Camire J, Keller J (1996) Low-pressure vortex tubes. J Phys D Appl Phys 29:1469
4. Ahlborn B, Keller J, Rebhan E (1998) The heat pump in a vortex tube. J Non-Equilib Thermodyn 23:159–165
5. Aljuwayhel N, Nellis G, Klein S (2005) Parametric and internal study of the vortex tube using a CFD model. Int J Refrig 28:442–450
6. Alsaghir AM, Hamdan MO, Orhan MF (2021) Evaluating velocity and temperature fields for Ranque–Hilsch vortex tube using numerical simulation. Int J Thermofluids 10:100074
7. Alsaghir AM, Hamdan MO, Orhan MF, Awad M (2022) Numerical and sensitivity analyses of various design parameters to maximize performance of a vortex tube. Int J Thermofluids 13:100133
8. Alsayyed B, Hamdan MO, Aldajah S (2012) Vortex tube impact on cooling milling machining. In: ASME international mechanical engineering congress and exposition. American Society of Mechanical Engineers, New York, pp 773–776
9. Ansys C (2006) Solver theory guide. Ansys CFX Release 11:1996–2006
10. Aydın O, Baki M (2006) An experimental study on the design parameters of a counterflow vortex tube. Energy 31:2763–2772
11. Bazgir A, Nabhani N (2018) Investigation of temperature separation inside various models of Ranque–Hilsch vortex tube: convergent, straight, and divergent with the help of computational fluid dynamic approach. J Therm Sci Eng Appl. https://doi.org/10.1115/1.4039966
12. Bazgir A, Heydari A, Nabhani N (2019) Investigation of the thermal separation in a counter-flow Ranque–Hilsch vortex tube with regard to different fin geometries located inside the cold-tube length. Int Commun Heat Mass Transf 108:104273
13. Bianco V, Khait A, Noskov A, Alekhin V (2016) A comparison of the application of RSM and LES turbulence models in the numerical simulation of thermal and flow patterns in a double-circuit Ranque–Hilsch vortex tube. Appl Therm Eng 106:1244–1256
14. Cartlidge J, Chowdhury N, Povey T (2022) Performance characteristics of a divergent vortex tube. Int J Heat Mass Transf 186:122497
15. Cengel YA (2010) Fluid mechanics. Tata McGraw-Hill Education, New Delhi
16. Cengel Y, Heat TM (2003) A practical approach. McGraw-Hill, New York, NY, USA
17. Deissler R, Perlmutter M (1960) Analysis of the flow and energy separation in a turbulent vortex. Int J Heat Mass Transf 1:173–191
18. Devade KD, Pise AT (2017) Effect of Mach number, valve angle and length to diameter ratio on thermal performance in flow of air through Ranque Hilsch vortex tube. Heat Mass Transf 53:161–168
19. Fulton CD (1950) Ranque's tube. J ASRE Refrig Eng 48:473–479
20. Gao C (2005) Experimental study on the Ranque–Hilsch vortex tube. Cryogenics 45(3):173–183
21. Guo X, Zhang B (2018) Computational investigation of precessing vortex breakdown and energy separation in a Ranque–Hilsch vortex tube. Int J Refrig 85:42–57
22. Gutsol A (1997) The ranque effect. Phys Usp 40:639
23. Hamdan MO, Alawar A, Elnajjar E, Siddique W (2011) Feasibility of vortex tube air-conditioning system. In: ASME/JSME 2011 8th thermal engineering joint conference. American Society of Mechanical Engineers Digital Collection. American Society of Mechanical Engineers, New York
24. Hamdan MO, Alsayyed B, Elnajjar E (2013) Nozzle parameters affecting vortex tube energy separation performance. Heat Mass Transf 49:533–541
25. Han X, Li N, Wu K, Wang Z, Tang L, Chen G, Xu X (2013) The influence of working gas characteristics on energy separation of vortex tube. Appl Therm Eng 61:171–177
26. Hilsch R (1947) The use of the expansion of gases in a centrifugal field as cooling process. Rev Sci Instrum 18:108–113
27. Hu Z, Li R, Yang X, Yang M, Day R, Wu H (2020) Energy separation for Ranque-Hilsch vortex tube: A short review. Therm Sci Eng Prog 19:100559
28. Khait A, Noskov A, Alekhin V, Bianco V (2018) Analysis of the local entropy generation in a double-circuit vortex tube. Appl Therm Eng 130:1391–1403

29. Khazaei H, Teymourtash AR, Malek-Jafarian M (2012) Effects of gas properties and geometrical parameters on performance of a vortex tube. Sci Iran 19:454–462

30. Kurosaka M (1982) Acoustic streaming in swirling flow and the Ranque—Hilsch (vortex-tube) effect. J Fluid Mech 124:139–172

31. Liang F, Wang H, Tang G (2020) Temperature separation characteristics of CH_4–CO_2 binary gas mixture within a vortex tube. Int J Therm Sci 161:106726

32. Liang F, Zeng Q, Tang G, Xin L, Li Q, Li N (2022) Numerical investigation on the effect of convergent-divergent tube on energy separation characteristic of vortex tube. Int Commun Heat Mass Transfer 133:105927

33. Niknam PH, Mortaheb H, Mokhtarani B (2017) Numerical investigation of a Ranque–Hilsch vortex tube using a three-equation turbulence model. Chem Eng Commun 204:327–336

34. O'Connell JP (2018) Detailed thermodynamics for analysis and design of Ranque–Hilsch vortex tubes. AIChE J 64:1067–1074

35. Ranque G (1933) Experiments on expansion in a vortex with simultaneous exhaust of hot air and cold air. J Phys Radium 4:112–114

36. Saidi M, Valipour M (2003) Experimental modeling of vortex tube refrigerator. Appl Therm Eng 23:1971–1980

37. Stephan K, Lin S, Durst M, Huang F, Seher D (1984) A similarity relation for energy separation in a vortex tube. Int J Heat Mass Transf 27:911–920

38. Wang Z, Suen K (2020) Numerical comparisons of the thermal behaviour of air and refrigerants in the vortex tube. Appl Therm Eng 164:114515